Available online at www.sciencedirect.com

ScienceDirect

Advances in Space Research xx (2022) xxx-xxx

ADVANCES IN SPACE RESEARCH (a COSPAR publication)

www.elsevier.com/locate/asr

Intelligent Selection of NEO Deflection Strategies Under Uncertainty

Yirui Wang[a,b], Massimiliano Vasile[a,*]

[a]Aerospace Centre of Excellence, University of Strathclyde, 75 Monterose Street, G11XJ, Glasgow, United Kingdom
[b]National Space Science Center, Chinese Academy of Sciences, NO.1 Nanertiao, 100190, Beijing, China

Received 1 May 2022; Received in final form 10 May 2022; Accepted 13 May 2022;
Available online 15 May 2022

Abstract

This paper presents an Intelligent Decision Support System (IDSS) that can automatically assess the suitable robust deflection strategies to respond to an asteroid impact scenario. The input to the IDSS is the warning time, the orbital parameters and mass of the asteroid and the corresponding uncertainties. The output is the deflection strategies that are more likely to offer a successful deflection. Both aleatory and epistemic uncertainties on ephemerides and physical properties of the asteroid are considered.

The training data set is produced by generating thousands of virtual impactors, sampled from the current distribution of Near Earth Objects (NEO). For each virtual impactor we perform a robust optimisation, under mixed aleatory/epistemic uncertainties, of the deflection scenario with different deflection strategies. The robust performance indices is considered by the deflection effectiveness, which is quantified by Probability of Collision post deflection. The IDSS is based on a combination Dempster-Shafer theory of evidence and a Random Forest classifier that is trained on the data set of virtual impactors and deflection scenarios. Five deflection strategies are modelled and included in the IDSS: Nuclear Explosion, Kinetic Impactor, Laser Ablation, Gravity Tractor and Ion Beam Shepherd. Simulation results suggest that the proposed decision support system can quickly provide robust decisions on which deflection strategies are to be chosen to respond to a NEO impact scenario. Once trained the IDSS does not require re-running expensive simulations to make decisions on which deflection strategies are to be used and is, therefore, suitable for the rapid pre-screening or reassessment of deflection options.

Keywords: Asteroid Deflection; Aleatory/Epistemic Uncertainty; Robust Optimisation; Machine Learning

1. Introduction

Asteroid impact poses a major threaten to all life forms on Earth. Several serious impact events through history, from the Chixulub Event 66 million years ago, to the Tunguska Event in 1908 down to the more recent Chelyabinsk Event in 2013, have concretely demonstrated the risk of an impact with asteroids and comets. In order to mitigate this risk, a number of remediation actions have been proposed over the year. Some of them consist of deflecting the NEO to avoid an impact with Earth. Most deflection strategies can be divided into two categories: impulsive methods (such as Nuclear Explosions Device Vasile & Thiry (2016), Kinetic Impactor

*Corresponding author: Massimiliano.vasile@strath.ac.uk

https://dx.doi.org/10.1016/j.jasr.xxxx.xx.xxx

Vasile & Colombo (2008)) and Slow-push methods (such as Laser ablation Zuiani et al. (2012a), Gravitational Tractor Lu & Love (2005), Ion Beam Shepherd Bombardelli et al. (2013)). Previous studies Sanchez et al. (2009); Thiry & Vasile (2017); Weisbin et al. (2015) compared the performance of different deflection strategies under the assumption of complete knowledge of the asteroid and the deflection outcome.

However, in the planning and decision making process that precedes the implementation of an asteroid deflection mission, there is a considerable amount of uncertainty affecting any decision Dearborn et al. (2020). In addition to the aleatory uncertainties which derive from the inherent randomness that is inevitable, the epistemic uncertainty, coming from the lack of knowledge and limited experimental opportunities, cannot be ignored. Previous studies Zuiani et al. (2012a) showed that by including epistemic uncertainties in the optimisation process, one can observe that in the worst case scenario the effectiveness of the whole concept can be severely compromised. The uncertainty factors will make the optimal solution, which is obtained under deterministic assumptions, become sub-optimal solution or even infeasible. For this reason, a number of past studies Vasile (2002); Yamaguchi et al. (2008); Paek et al. (2020) proposed robust optimisation methods for asteroid deflection missions. Computing a robust and globally optimal solution under mixed aleatory and epistemic uncertainty is computationally expensive and the cost rapidly grows with the number of uncertain quantities. The cost further increases with the fidelity of the deflection action and associated uncertainty model. Furthermore, making decisions on the optimal response to a threat scenario requires accounting for different factors, including the available time to implement a deflection action and the orbital elements of the asteroid, which affect the transfer time and cost. At the same time the development of a deflection mission is expected to go through different phases of growing complexity in which the appropriateness of a deflection action has to be re-assessed multiple times given the level of uncertainty and maturity of the deflection technology and the knowledge of the target NEO. Thus making optimal decisions, especially in the preliminary phase, requires a proper treatment of both aleatory and epistemic uncertainty and a way to quickly assess the appropriateness of a technology under uncertainty.

This paper proposes an Intelligent Decision Support System (IDSS) based on a combination of ML and Dempster-Shaffer theory of evidence (DSt) to handle epistemic uncertainty. A ML model is trained on a data-set of virtual impactors, deflection scenarios and deflection technologies with associated uncertainty. Once trained, the ML model works like an oracle that can be interrogated multiple times to assess which deflection methods is to be used in response to a threatening scenario. In this context, Machine Learning provides a way to make robust decisions under uncertainty without the need of multiple runs of expensive mission and system design optimisations. The ML model encapsulates different processes that concur to assess which deflection strategies are likely to offer a successful deflection: computation of the deflection action, transfer trajectory definition, quantification of system and NEO uncertainty, optimisation of the deflection mission. DSt adds a further important layer to the decision process by quantifying the uncertainty deriving from a lack of knowledge on the NEO, the deflection action and the deflection technology. The use of Machine Learning has found a growing range of application in the space sector in the last decade. However, its application in the field of Planetary Defense (PD) is still limited. Recent examples include the selection of asteroid deflection strategy Nesvold et al. (2018), a PD Resource Discovery Engine Bambacus et al. (2017), and the estimation of momentum transfer factor β from experimentsRaskin et al. (2021). Meanwhile, a decision support system for space traffic management was proposed by the authors to provide operators with automatic collision avoidance capabilities Sánchez Fernández-Mellado & Vasile (2021). The IDSS in this paper is conceptually derived from Sánchez Fernández-Mellado & Vasile (2021) and differentiates itself from the Deflector Selector proposed in Nesvold et al. (2018) in three different ways: i) it takes both aleatory and epistemic uncertainty affecting the deflection action as an input and uses DSt to quantify the uncertainty in the probability of an impact, ii) it extends the range of deflection technologies to be considered, ii) it introduces a robustness criterion on the success of the deflection action to allow making robust decisions under uncertainty.

The paper is structured as follows. Section 2 will introduce the general methodology we proposed, while section 3 will describe the IDSS and present some preliminary results.

2. Methodology

This section will briefly introduce the proposed methodology and the approach to uncertainty quantification and propagation. Then it will present the models used to compute both impulsive and slow push deflections and finally it will describe the approach

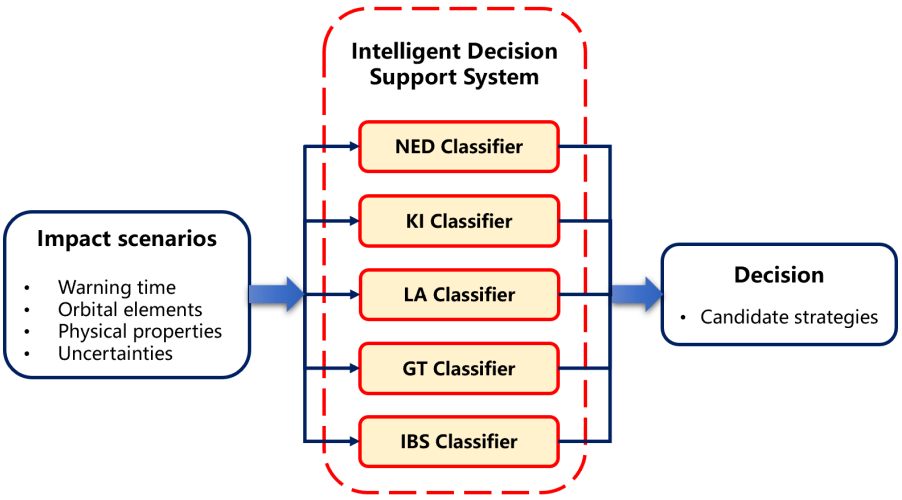

Fig. 1: Architecture of Intelligent Decision Support System (IDSS). The input of IDSS includes the information of impact scenarios, such as warning time, orbital elements, size and corresponding uncertainties. IDSS consists of five sub-classifiers, which can automatically output if the corresponding deflection strategies can provide a successful deflection.

we propose to compute robust and optimal deflection solutions.

Figure 1 shows a diagram representing the overall architecture of the proposed IDSS. The core of the IDSS is composed of five classifiers one for each of the deflection actions considered in this paper: Nuclear Explosion Device (NED), Kinetic Impactor (KI), Laser Ablation (LA), Gravity Tractor (GT) and Ion Beam Shepherd (IBS). Additional deflection technologies can be included through other classifiers. The input to the IDSS is the warning time, the orbital parameters of the NEO and a number of uncertainty sources on the physical properties of the NEO and the technologies to be used. In this paper, as a preliminary demonstration, we considered only the diameter of the NEO, with associated uncertainty, and the uncertainty on its ephemerides. The output of each classifier is a label that says if the corresponding method can achieve a successful deflection or not. Thus the overall output of the IDSS is a number of methods that are expected to be successfully applicable to the input scenario.

2.1. Uncertainty quantification and propagation

In this paper, we consider a mix of aleatory and epistemic uncertainties affecting the knowledge of the position of the NEO at time of closest approach with the Earth. More specifically, we modelled the uncertainty in the ephemerides and visual magnitude of the NEO with a family of Gaussian distributions where the mean and variance are effected by epistemic uncertainty. The assumption is that the true value of the orbital elements $\tilde{\mathbf{æ}} = \left[\tilde{a}, \tilde{e}, \tilde{i}, \tilde{\Omega}, \tilde{\omega}, \tilde{M}\right]^T$ and absolute visual magnitude $\tilde{H}$ can be defined as:

$$\tilde{\mathbf{æ}} = \mathbf{æ} + \Delta\mathbf{æ} \tag{1}$$

$$\tilde{H} = H + \Delta H \tag{2}$$

where $\mathbf{æ} = [a, e, i, \Omega, \omega, M, H]^T$ and H are expected values, $\Delta\mathbf{æ} = [\Delta a, \Delta e, \Delta i, \Delta\Omega, \Delta\omega, \Delta M]$ and ΔH are the corresponding uncertainties. Absolute visual magnitude H Chesley et al. (2002) will be used for estimating the mass of the asteroid (assuming the asteroid's density ρ is 2.6 g/cm^3, albedo p is 0.154)

$$\begin{cases} D = \frac{1329}{10^{0.2H}\sqrt{p}} \\ m_{\mathrm{Ast}} = \frac{1}{6}\pi D^3 \rho \end{cases} \tag{3}$$

Let $\boldsymbol{\lambda_{\text{æ}}}$ and $\boldsymbol{\lambda}_H$ be two parameter vectors defining the uncertainty models $\Delta\boldsymbol{\text{æ}}(\boldsymbol{\lambda_{\text{æ}}})$ and $\Delta H(\boldsymbol{\lambda}_H)$, the expected values $\boldsymbol{\text{æ}} = \boldsymbol{\mu}^T_{\boldsymbol{\text{æ}}}$ and $H = \mu^T_H$. Then, $\tilde{\boldsymbol{\text{æ}}}$ and $\tilde{H}$ under mixed aleatory and epistemic uncertainties are expressed as:

$$\begin{aligned} \tilde{\boldsymbol{\text{æ}}} &= \boldsymbol{\mu}^T_{\boldsymbol{\text{æ}}} + \Delta\boldsymbol{\text{æ}}\,(\boldsymbol{\lambda_{\text{æ}}}) \\ \tilde{H} &= \mu^T_H + \Delta H\,(\boldsymbol{\lambda}_H) \end{aligned} \tag{4}$$

with $\boldsymbol{\lambda_{\text{æ}}}$ and $\boldsymbol{\lambda_H}$ subject to the conditions $\boldsymbol{\lambda_{\text{æ}}} \in [\underline{\boldsymbol{\lambda_{\text{æ}}}}, \overline{\boldsymbol{\lambda_{\text{æ}}}}]$ and $\boldsymbol{\lambda_H} \in [\underline{\boldsymbol{\lambda_H}}, \overline{\boldsymbol{\lambda_H}}]$. In the following the values $\Delta\boldsymbol{\text{æ}}$ and ΔH are drawn from two normal distributions $N(0, \boldsymbol{\sigma}^T_{\boldsymbol{\text{æ}}})$ and $N(0, \sigma^T_H)$ respectively, thus $\overline{\boldsymbol{\lambda}}_{\boldsymbol{\text{æ}}} = \boldsymbol{\sigma}^T_{\boldsymbol{\text{æ}}}$ and $\boldsymbol{\lambda}_H = \sigma^T_H$. The covariance matrix of the orbital elements $\boldsymbol{\Sigma}_{\boldsymbol{\text{æ}}}$ at the initial state is defined as a diagonal matrix

$$\boldsymbol{\Sigma}_{\text{æ}} = \boldsymbol{A}\boldsymbol{A}^{\mathrm{T}}, \quad \boldsymbol{A} = diag\,(\sigma_a, \sigma_e, \sigma_i, \sigma_\Omega, \sigma_\omega, \sigma_M) \tag{5}$$

Dempster-Shafer theory of evidence (DSt) Shafer (1976), known also as the Evidence Theory, is a mathematical framework to model epistemic uncertainty and can be interpreted as a generalisation of classical probability theory. DSt can be used to model both aleatory and epistemic uncertainty in NEO properties and deflection technology as shown in Zuiani et al. (2012a). In this paper we will use DSt to model the epistemic uncertainty in $\boldsymbol{\lambda_{\text{æ}}}$ and $\boldsymbol{\lambda_H}$, and assess the uncertainty in the objective function accounting for all available pieces of evidence.

For every value of the uncertain parameters $\boldsymbol{\lambda_{\text{æ}}}$ and $\boldsymbol{\lambda_H}$, the Unscented Transform (UT) Julier et al. (1995) is used to propagate the expected value and aleatory uncertainty in $\tilde{\boldsymbol{\text{æ}}}$ and $\tilde{H}$. UT was proposed to calculate the mean value and the covariance matrix of a random variable that undergoes a nonlinear transformation. The basic idea is that, instead of performing a higher order analysis, the probability distribution parameters at a future time can be approximated by using a set of representative points, called sigma points Luo & Yang (2017).

2.2. Deflection Methods

This section briefly describes the proposed approach to model the achievable deflection with both impulsive and slow-push deflection actions. The change of linear momentum induced by each deflection action is modelled as in Vasile & Thiry (2016) and Thiry & Vasile (2017). All the models in Vasile & Thiry (2016) and Thiry & Vasile (2017) are low fidelity and parametric. Thus they allow one to compute the change of linear momentum analytically and to introduce uncertainty in the deflection action through the parameters of the models.

2.2.1. Impulsive methods

The effect of an impulsive change in the velocity of the asteroid induces a variation of its orbital elements. According to the method proposed in Ref. Vasile & Colombo (2008), the deflection position on the B-plane can be calculated analytically by rewriting $\delta\boldsymbol{v}$ in a tangential, normal, out-of-plane reference frame

$$\delta\boldsymbol{v} = [\delta v_t, \delta v_n, \delta v_h]^{\mathrm{T}} \tag{6}$$

The variation of Keplerian elements at the time of deflection t_d caused by $\delta \boldsymbol{v}$ can be calculated by

$$\begin{aligned}
\delta a &= \frac{2\tilde{a}^2\tilde{v}}{\mu}\delta v_t \\
\delta e &= \frac{1}{\tilde{v}}\left[2\left(\tilde{e}+\cos\tilde{\theta}_d\right)\delta v_t - \frac{\tilde{r}}{\tilde{a}}\sin\tilde{\theta}_d\delta v_n\right] \\
\delta i &= \frac{\tilde{r}\cos\tilde{\theta}_d^*}{\tilde{h}}\delta v_h \\
\delta\Omega &= \frac{\tilde{r}\sin\tilde{\theta}_d^*}{\tilde{h}\sin\tilde{i}}\delta v_h \\
\delta\omega &= \frac{1}{\tilde{e}\tilde{v}}\left[2\sin\tilde{\theta}_d\delta v_t + (2e+\frac{\tilde{r}}{\tilde{a}}\cos\tilde{\theta}_d)\delta v_n\right] - \frac{\tilde{r}\sin\tilde{\theta}_d^*\cos\tilde{i}}{\tilde{h}\sin\tilde{i}}\delta v_h \\
\delta M_d &= -\frac{\tilde{b}}{\tilde{e}\tilde{a}\tilde{v}}\left[2\left(1+\frac{\tilde{e}^2\tilde{r}}{\tilde{p}}\right)\sin\tilde{\theta}_d\delta v_t + \frac{\tilde{r}}{\tilde{a}}\cos\tilde{\theta}_d\delta v_n\right]
\end{aligned} \tag{7}$$

due to the change of semi-major axis, the change in the mean anomaly at the collision time t_{MOID} is given by

$$\delta M_n = \delta n\Delta t = \left(\sqrt{\frac{\mu}{\tilde{a}^3}} - \sqrt{\frac{\mu}{(\tilde{a}+\delta a)^3}}\right)(t_{\mathrm{MOID}} - t_d) \tag{8}$$

therefore, the total variation in the mean anomaly δM between the unperturbed and the deflected orbit is

$$\delta M = \delta M_d + \delta M_n \tag{9}$$

The position of the deflected asteroid with respect to the undeflected one at the true anomaly θ_{MOID} along the orbit of the undeflected asteroid is Schaub & Junkins (2003):

$$\begin{aligned}
\delta x_r &\approx \frac{\tilde{r}}{\tilde{a}}\delta a + \frac{\tilde{a}\tilde{e}\sin\theta_{\mathrm{MOID}}}{\sqrt{1-\tilde{e}^2}}\delta\tilde{M} - a\cos\tilde{\theta}_{\mathrm{MOID}}\delta\tilde{e} \\
\delta y_\theta &\approx \frac{\tilde{r}}{\left(1-\tilde{e}^2\right)^{3/2}}\left(1+\tilde{e}\cos\tilde{\theta}_{\mathrm{MOID}}\right)^2\delta\tilde{M} + \tilde{r}\delta\tilde{\omega} + \frac{\tilde{r}\sin\tilde{\theta}_{\mathrm{MOID}}}{(1-\tilde{e})}\left(2+\tilde{e}\cos\tilde{\theta}_{\mathrm{MOID}}\right)\delta\tilde{e} + \tilde{r}\cos\tilde{i}\delta\tilde{\Omega} \\
\delta z_h &\approx \tilde{r}\left(\sin\tilde{\theta}^*_{\mathrm{MOID}}\delta\tilde{i} - \cos\tilde{\theta}^*_{\mathrm{MOID}}\sin\tilde{i}\delta\tilde{\Omega}\right)
\end{aligned} \tag{10}$$

where $\delta\boldsymbol{r} = [\delta x_r, \quad \delta y_\theta, \quad \delta z_h]^{\mathrm{T}}$ is the deflection vector at the collision time t_{MOID} in a radial, transverse, out-of-plane reference frame attached to the undeflected asteroid. In short, the deflection vector $\delta\boldsymbol{r}\left(\delta\boldsymbol{v}, t_d; \boldsymbol{\mathfrak{a}}, \Delta\boldsymbol{\mathfrak{a}}\right)$ at collision time t_{MOID} after the impulsive strategy can be expressed as

$$\delta\boldsymbol{r} = \boldsymbol{A}_{\mathrm{MOID}}\delta\tilde{\boldsymbol{\mathfrak{a}}} \tag{11}$$

where $\delta\tilde{\boldsymbol{\mathfrak{a}}} = \left[\delta\tilde{a}, \delta\tilde{e}, \delta\tilde{i}, \delta\tilde{\Omega}, \delta\tilde{\omega}, \delta\tilde{M}\right]^T = \delta\boldsymbol{\mathfrak{a}} + \Delta\boldsymbol{\mathfrak{a}}$ indicates the total variation of orbital elements at t_{MOID}, $\Delta\boldsymbol{\mathfrak{a}}$ indicates the uncertainty of orbital elements, and $\boldsymbol{A}_{\mathrm{MOID}}$ indicates the transition matrix extracted from Eq.(10).

2.2.2. Slow-push methods

In the general case of slow-push strategies, the variation of orbital elements is computed by numerical integration of Gauss equations from the time t_d when the deflection action starts until the time t_f when the deflection action stops, considering the thrust acceleration as a perturbing acceleration. However, calculating the variation of orbital elements by numerical integration will be rather computationally expensive as thousands of trajectories need to be evaluated under the consideration of uncertainties. An approximated analytical solution of Gauss equations over short arcs for a constant thrust Zuiani et al. (2012b), which is named as Finite Perturbative Elements in Time (FPET), had been applied for the propagation of the motion of an asteroid under the effect of the slow-push deflection strategy Zuiani et al. (2012a), and the simulation results show that the computational time is at least one order of magnitude lower than numerical integration. In the reminder of this section we will give a brief introduction of FPET. The

variation of the orbital elements is obtained by integrating Gauss equations in non-singular equinoctial elements:

$$\begin{aligned}
\frac{da}{dt} &= \frac{2}{B}\sqrt{\frac{\tilde{a}^3}{\mu}}\left[\left(\tilde{P}_2\sin\tilde{L}-\tilde{P}_1\cos\tilde{L}\right)a_r+\Phi(\tilde{L})a_\theta\right]\\
\frac{dP_1}{dt} &= B\sqrt{\frac{\tilde{a}}{\mu}}\left[-a_r\cos\tilde{L}+\left(\frac{\tilde{P}_1+\sin\tilde{L}}{\Phi(\tilde{L})}+\sin\tilde{L}\right)a_\theta-\tilde{P}_2\frac{\tilde{Q}_1\cos\tilde{L}-\tilde{Q}_2\sin\tilde{L}}{\Phi(\tilde{L})}a_h\right]\\
\frac{dP_2}{dt} &= B\sqrt{\frac{\tilde{a}}{\mu}}\left[a_r\sin\tilde{L}+\left(\frac{\tilde{P}_2+\cos\tilde{L}}{\Phi(\tilde{L})}+\cos\tilde{L}\right)a_\theta+\tilde{P}_1\frac{\tilde{Q}_1\cos\tilde{L}-\tilde{Q}_2\sin\tilde{L}}{\Phi(\tilde{L})}a_h\right]\\
\frac{dQ_1}{dt} &= \frac{B}{2}\sqrt{\frac{\tilde{a}}{\mu}}\left(1+\tilde{Q}_1^2+\tilde{Q}_2^2\right)\frac{\sin\tilde{L}}{\Phi(\tilde{L})}a_h\\
\frac{dQ_2}{dt} &= \frac{B}{2}\sqrt{\frac{\tilde{a}}{\mu}}\left(1+\tilde{Q}_1^2+\tilde{Q}_2^2\right)\frac{\cos\tilde{L}}{\Phi(\tilde{L})}a_h
\end{aligned} \tag{12}$$

where L is the true longitude, $B=\sqrt{1+\tilde{P}_1^2+\tilde{P}_2^2}$, $\Phi(\tilde{L})=1+\tilde{P}_1\sin\tilde{L}+\tilde{P}_2\cos\tilde{L}$, and

$$\begin{aligned}
\tilde{P}_1 &= \tilde{e}\sin(\tilde{\Omega}+\tilde{\omega})\\
\tilde{P}_2 &= \tilde{e}\cos(\tilde{\Omega}+\tilde{\omega})\\
\tilde{Q}_1 &= \tan(\frac{\tilde{i}}{2})\sin(\tilde{\Omega})\\
\tilde{Q}_2 &= \tan(\frac{\tilde{i}}{2})\cos(\tilde{\Omega})\\
\tilde{L} &= \tilde{\Omega}+\tilde{\omega}+\tilde{\theta}
\end{aligned} \tag{13}$$

The components of thrust vector is formed by modulus ϵ, azimuth α and elevation β of the thrust acceleration in the radial-transverse reference frame:

$$\boldsymbol{f}=[a_r \quad a_\theta \quad a_h]=\epsilon\left[\cos\alpha\cos\beta \quad \sin\alpha\cos\beta \quad \sin\beta\right]^T \tag{14}$$

If one assumes that the modulus of the perturbing acceleration is small compared to the local gravitational acceleration, then

$$\frac{dt}{dL}\approx\sqrt{\frac{\tilde{a}^3}{\mu}}\frac{B^3}{\Phi^2(\tilde{L})} \tag{15}$$

By substituting Eq.14 and Eq.15 into Eq.12 , the system of equations in the longitude L can be summarized in a vector form as

$$\frac{d\boldsymbol{E}}{dL}=\epsilon F(\tilde{\boldsymbol{E}},\tilde{L},\alpha,\beta) \tag{16}$$

where $\tilde{\boldsymbol{E}}=[\tilde{a},\tilde{P}_1,\tilde{P}_2,\tilde{Q}_1,\tilde{Q}_2]^T$. The solution of Eq.16 can be expanded to the first order in the perturbing parameter ϵ

$$\tilde{\boldsymbol{E}}(\tilde{L})\approx\tilde{\boldsymbol{E}}_{\boldsymbol{0}}(\tilde{L}_0)+\epsilon\tilde{\boldsymbol{E}}_{\boldsymbol{1}}(\Delta\tilde{L},\alpha,\beta)+O(\epsilon^2) \tag{17}$$

where $\tilde{L}=\tilde{L}_0+\Delta\tilde{L}$. By substituting Eq.17 into Eq.16 and expanding the right hand side in Taylor series with respect to ϵ, collecting the terms which depend on the same power of ϵ, then, the $\boldsymbol{E_0}$ and $\boldsymbol{E_1}$ can be expressed as

$$\begin{cases}
\tilde{\boldsymbol{E}}_{\boldsymbol{0}} = const\\
\tilde{\boldsymbol{E}}_{\boldsymbol{1}} = \int_{\tilde{L}_0}^{\tilde{L}} F(\tilde{\boldsymbol{E}}_{\boldsymbol{0}},\mathcal{L},\alpha,\beta)\,d\mathcal{L}
\end{cases} \tag{18}$$

The keplerian elements can be transformed by the equinoctial elements, therefore, the variation of the keplerian elements due to the slow-push action can be obtained

$$\tilde{\boldsymbol{E}}(\tilde{L_f}) - \tilde{\boldsymbol{E}}(\tilde{L_d}) \Rightarrow \tilde{\boldsymbol{æ}}(t_f) - \tilde{\boldsymbol{æ}}(t_d) = \delta\tilde{\boldsymbol{æ}} = \left[\delta\tilde{a}, \delta\tilde{e}, \delta\tilde{i}, \delta\tilde{\Omega}, \delta\tilde{\omega}, \delta\tilde{M}\right]^T \tag{19}$$

Furthermore, the total variation in the mean anomaly between deflected and undeflected orbit is

$$\delta\tilde{M} = \tilde{M}'_{\mathrm{MOID}} - \tilde{M}_{\mathrm{MOID}} = [\tilde{M}_d + \delta M_d + \tilde{n}_f(t_{\mathrm{MOID}} - t_f)] - [\tilde{M}_d + \tilde{n}_d(t_{\mathrm{MOID}} - t_d)] \tag{20}$$

Therefore, the deflection vector $\delta\boldsymbol{r}\left(\boldsymbol{f}, t_d, t_f; \boldsymbol{æ}, \Delta\boldsymbol{æ}\right)$ after the slow-push strategy can be calculated by Eq. (11).

2.2.3. Projection on the B-Plane

Once the deflection vector $\delta\boldsymbol{r}$ is calculated, the corresponding vector in the B-plane coordinates $\tilde{\boldsymbol{x}}_b$ can be expressed in terms of the asteroid's heliocentric position $\boldsymbol{r}_{\mathrm{Ast}}(t_{\mathrm{MOID}})$, heliocentric velocity $\boldsymbol{v}_{\mathrm{Ast}}(t_{\mathrm{MOID}})$ and the geocentric velocity $\boldsymbol{U}(t_{\mathrm{MOID}})$:

$$\tilde{\boldsymbol{x}}_b\left(t_{\mathrm{MOID}}\right) = \left[\hat{\boldsymbol{\xi}} \quad \hat{\boldsymbol{\eta}} \quad \hat{\boldsymbol{\zeta}}\right]^{\mathrm{T}}\left[\hat{\boldsymbol{r}} \quad \hat{\boldsymbol{\theta}} \quad \hat{\boldsymbol{h}}\right]\delta\boldsymbol{r} \tag{21}$$

where $\hat{\boldsymbol{r}}, \hat{\boldsymbol{\theta}}, \hat{\boldsymbol{h}}$ are column vectors that define the radial, transverse, out-of-plane reference frame:

$$\hat{\boldsymbol{r}} = \frac{\boldsymbol{r}_{\mathrm{Ast}}\left(t_{\mathrm{MOID}}\right)}{\|\boldsymbol{r}_{\mathrm{Ast}}\left(t_{\mathrm{MOID}}\right)\|}, \quad \hat{\boldsymbol{h}} = \frac{\boldsymbol{r}_{\mathrm{Ast}}\left(t_{\mathrm{MOID}}\right) \times \boldsymbol{v}_{\mathrm{Ast}}\left(t_{\mathrm{MOID}}\right)}{\|\boldsymbol{r}_{\mathrm{Ast}}\left(t_{\mathrm{MOID}}\right) \times \boldsymbol{v}_{\mathrm{Ast}}\left(t_{\mathrm{MOID}}\right)\|}, \hat{\boldsymbol{\theta}} = \frac{\hat{\boldsymbol{h}} \times \hat{\boldsymbol{r}}}{\|\hat{\boldsymbol{h}} \times \hat{\boldsymbol{r}}\|} \tag{22}$$

$\hat{\boldsymbol{\xi}}, \hat{\boldsymbol{\eta}}, \hat{\boldsymbol{\zeta}}^{\mathrm{T}}$ are column vectors that define the B-plane reference frame:

$$\hat{\boldsymbol{\eta}} = \frac{\boldsymbol{U}\left(t_{\mathrm{MOID}}\right)}{\|\boldsymbol{U}\left(t_{\mathrm{MOID}}\right)\|}, \quad \hat{\boldsymbol{\xi}} = \frac{\boldsymbol{v}_E\left(t_{\mathrm{MOID}}\right) \times \hat{\boldsymbol{\xi}}}{\|\boldsymbol{v}_E\left(t_{\mathrm{MOID}}\right) \times \hat{\boldsymbol{\xi}}\|}, \quad \hat{\boldsymbol{\zeta}} = \frac{\hat{\boldsymbol{\xi}} \times \hat{\boldsymbol{\eta}}}{\|\hat{\boldsymbol{\xi}} \times \hat{\boldsymbol{\eta}}\|} \tag{23}$$

The deflection distance of the deflection action is measured by the projection of the deflection vector $\delta\boldsymbol{r}$ on the B-plane as

$$\tilde{\boldsymbol{b}} = \left[\tilde{x}_{b\xi}, \tilde{x}_{b\zeta}\right]^T \tag{24}$$

Once the mean value and standard deviation of asteroid orbital elements and magnitude are given at the deflection time t_d, the mean value $\boldsymbol{\mu}_{\xi\zeta}$ and covariance matrix $\boldsymbol{\mu}_{\xi\zeta}$ of $\tilde{\boldsymbol{b}}$ can be approximated by aforementioned UT technique as the following steps: The $\tilde{\boldsymbol{b}}$ should be reformed as a function $\boldsymbol{\mathcal{T}}$ of orbital elements $\tilde{\boldsymbol{æ}}$ and the magnitude $\tilde{H}$.

$$\tilde{\boldsymbol{b}} = \boldsymbol{\mathcal{T}}\left(\tilde{\boldsymbol{X}}\right), \quad \tilde{\boldsymbol{X}} = \left[\tilde{a}, \tilde{e}, \tilde{i}, \tilde{\Omega}, \tilde{\omega}, \tilde{M}, \tilde{H}\right]^T \tag{25}$$

The mean value and covariance matrix of $\tilde{X}$ are

$$\begin{cases} \boldsymbol{\mu}_{\tilde{\boldsymbol{X}}} = [a, e, i, \Omega, \omega, M, H]^T \\ \boldsymbol{\Sigma}_{\tilde{\boldsymbol{X}}} = \boldsymbol{A}\boldsymbol{A}^{\mathrm{T}}, \quad \boldsymbol{A} = diag\left(\sigma_a, \sigma_e, \sigma_i, \sigma_\Omega, \sigma_\omega, \sigma_M, \sigma_H\right) \end{cases} \tag{26}$$

Calculate the sigma points $\boldsymbol{\mathcal{X}}$ and their weights $W_m^{(i)}, W_c^{(i)} (i = 0, 1, ..., 2n)$:

$$\begin{aligned} \boldsymbol{\mathcal{X}}^{(0)} &= \boldsymbol{\mu}_{\tilde{\boldsymbol{X}}}, \quad W_m^{(0)} = \frac{\lambda}{(n+\lambda)}, \quad W_c^{(0)} = W_m^{(i)} + (1 - \alpha^2 + \beta) \\ \boldsymbol{\mathcal{X}}^{(j)} &= \boldsymbol{\mu}_{\tilde{\boldsymbol{X}}} + \left(\sqrt{(n+\lambda)\boldsymbol{\Sigma}_{\tilde{\boldsymbol{X}}}}\right)_j, \quad W_m^{(j)} = \frac{1}{2(n+\lambda)}, \quad W_c^{(j)} = W_m^{(j)} \\ \boldsymbol{\mathcal{X}}^{(n+j)} &= \boldsymbol{\mu}_{\tilde{\boldsymbol{X}}} - \left(\sqrt{(n+\lambda)\boldsymbol{\Sigma}_{\tilde{\boldsymbol{X}}}}\right)_j, \quad W_m^{(n+j)} = \frac{1}{2(n+\lambda)}, \quad W_c^{(n+j)} = W_m^{(n+j)} \end{aligned} \tag{27}$$

where $j = 1, 2, ..., n; n \in \mathbb{N}$ is the dimension of the state vector; β should be 2 for Gaussian distributions; and $(\dots)_j$ means the j^{th} column vector of the matrix. Obtain the set of the transformed sigma points $\boldsymbol{\mathcal{Y}}^{(i)}$:

$$\boldsymbol{\mathcal{Y}}^{(i)} = \boldsymbol{\mathcal{T}}\left(\boldsymbol{\mathcal{X}}^{(i)}\right) \tag{28}$$

The mean value and the covariance are by using the weights and transformed sigma points as follows:

$$\boldsymbol{\mu}_{\xi\zeta} = \sum_{i=0}^{2n} W_c^{(i)} \boldsymbol{\mathcal{Y}} \tag{29}$$

$$\boldsymbol{\Sigma}_{\xi\zeta} = \sum_{i=0}^{2n} W_c^{(i)} \left[\boldsymbol{\mathcal{Y}}^{(i)} - \boldsymbol{\mu}_{\xi\zeta}\right]\left[\boldsymbol{\mathcal{Y}}^{(i)} - \boldsymbol{\mu}_{\xi\zeta}\right]^T \tag{30}$$

Therefore, the Probability of Collision P_c' after the deflection can be expressed as

$$P_c'\left(\boldsymbol{\mu}_{\xi\zeta}, \boldsymbol{\Sigma}_{\xi\zeta}\right) = \frac{1}{2\pi\sqrt{\left|\boldsymbol{\Sigma}_{\xi\zeta}\right|}} \iint_{\mathcal{B}((0,0),R)} e^{-\frac{1}{2}\left[(\tilde{\boldsymbol{b}}-\boldsymbol{\mu}_{\xi\zeta})^{\mathrm{T}}\boldsymbol{\Sigma}_{\xi\zeta}^{-1}(\tilde{\boldsymbol{b}}-\boldsymbol{\mu}_{\xi\zeta})\right]} d\xi\, d\zeta \tag{31}$$

where P_c' is computed by integrating the uncertainty ellipsoid, centered on the asteroid's mass point and projected on the B-plane, over the closed region $\mathcal{B}((0,0), R)$ defined by Earth's radius (assuming $R_E = 6378km$ in this paper). Patera's method Patera (2001) is used for calculating P_c' due to the fact that computational efficiency is particularly advantageous when large numbers of P_c' evaluations are performed.

2.3. Evidence-based Robust Optimisation

This paper proposes the use of the Probability of Collision after deflection P_c' as the objective function to quantify the deflection effectiveness:

$$f(\boldsymbol{d}, \boldsymbol{u}) = P_c' \tag{32}$$

where $\boldsymbol{d} \in D \subseteq \mathbb{R}^m$ is a decision vector defined over the decision space D and $\boldsymbol{u} \in U \subseteq \mathbb{R}^n$ is an epistemic uncertainty vector defined over the epistemic uncertainty space U. Since the uncertainties of asteroid's orbital elements and visual magnitude are considered in this paper, $\boldsymbol{u} = [\boldsymbol{\lambda_{\text{æ}}}, \lambda_H]^T$.

For NED, KI, LA missions, the decision vector $\boldsymbol{d}$ consists of two elements: the epoch of launch and the time of transfer. For GT and IBS missions, the decision vector $\boldsymbol{d}$ consists of three elements: the epoch of launch, the time of transfer and oversizing coefficient ([1, 10]) Thiry & Vasile (2017).

The deflection model accounts for the transfer time and cost as well as the mass of the deflection depends on the mass of the spacecraft and the time required to reach the asteroid. For impulsive methods, the transfer cost and time are obtained by solving Lambert's problem. For slow-push methods, the transfer cost and time are obtained by spherical shaping method Novak & Vasile (2011). The launch performance of Delta IV Heavy-RS-68A upgrade version is considered in the robust optimisation to define the initial mass of the spacecraft at the start of the transfer trajectory.

Following Dempster-Shafer theory of evidence the epistemic uncertainty in $\boldsymbol{\lambda_{\text{æ}}}$ and λ_H is modelled with intervals with associated Basic Probability Assignment (bpa). Consider for each component u_i of the uncertainty vector $\boldsymbol{u}$, a collection of s_i intervals:

$$I_i = \{e_{ij} | u_i \in e_{ij}, j = 1, ..., s_i\} \tag{33}$$

with a $bpa(e_{ij}) \in [0, 1]$ associated to each interval. Then the uncertainty set U is given by the Cartesian product $U = I_1 \times I_2 \times ... I_n$ and we can define a focal element $\gamma_q = e_{1J_q(1)} \times e_{2J_q(2)} \times ... e_{iJ_q(i)} \times ... e_{nJ_q(n)}$ with associated $bpa(\gamma_q) = \prod_i bpa_{iJ_q(i)}$ where the vector $\mathbf{J}_q$

has n components and contains a permutation of indexes j. We can now define the set A_ν as:

$$A_\nu = \{f(\boldsymbol{d},\boldsymbol{u}) | f(\boldsymbol{d},\boldsymbol{u}) < \nu, \boldsymbol{d} \in D, \boldsymbol{u} \in U\} \tag{34}$$

and the cumulative Belief and Plausibility associated to proposition in Eq.(34):

$$Bel(A_\nu) = \sum_{\gamma_q \subseteq A_\nu} bpa(\gamma_q) \tag{35}$$

$$Pl(A_\nu) = \sum_{\gamma_q \cap A_\nu \neq \varnothing} bpa(\gamma_q) \tag{36}$$

Once the Belief in a given value of ν is computed, the following multi-objective optimisation problem can be formulated in order to maximise the Belief in the minimum achievable P'_c:

$$\begin{aligned} &\max_{\boldsymbol{d}\in D} Bel\left(f\left(\boldsymbol{d},\boldsymbol{u}\right) < \nu\right) \\ &\min_{\boldsymbol{u}\in U} \nu \end{aligned} \tag{37}$$

The optimal design vector and thresholds that yield a $Bel = 1$ for all possible $\boldsymbol{u} \in U$ can be computed by solving the following classic min-max problem (optimizing 'worst case') Zuiani et al. (2012a):

$$\min_{\boldsymbol{d}\in D} \max_{\boldsymbol{u}\in U} f\left(\boldsymbol{d},\boldsymbol{u}\right) \tag{38}$$

Since the focal elements in U can be overlapping or disconnected, the calculation of $f\left(\boldsymbol{d},\boldsymbol{u}\right)$ needs to explore each focal element independently and therefore faces the solution of an exponential number of optimisation problems. If the goal is to solve problem (38), then the exponential complexity can be avoided by collecting all focal elements, through an affine transformation Vasile et al. (2011), into a compact unit hypercube $\overline{U}$ where all intervals along each dimension are adjacent and not overlapping. A point in the unit hypercube $\overline{U}$ is then mapped into the uncertainty space U through the simple affine transformation:

$$u_i = \frac{b^u_{U,i} - b^l_{U,i}}{b^u_{\overline{U},i} - b^l_{\overline{U},i}} \overline{u}_i + b^l_{U,i} - \frac{b^u_{U,i} - b^l_{U,i}}{b^u_{\overline{U},i} - b^l_{\overline{U},i}} b^l_{\overline{U},i} \tag{39}$$

where $b^u_{\overline{U},i}$ and $b^l_{\overline{U},i}$ are the upper and lower boundaries of the i-th interval to which $\overline{u}_i$ belongs and $b^u_{U,i}$ and $b^l_{U,i}$ are the upper and lower boundaries of the i-th interval to which u_i belongs. Problem (38) then becomes:

$$\min_{\boldsymbol{d}\in D} \max_{\overline{\boldsymbol{u}}\in \overline{U}} f\left(\boldsymbol{d},\overline{\boldsymbol{u}}\right) \tag{40}$$

Problem (40) is then solved with a nested loop. An inner loop maximises f over $\overline{U}$ while an outer loop minimises f over D. The Adaptive Multi-Population Inflationary Differential Evolution Algorithm (MP-AIDEA) Di Carlo et al. (2020) was used to globally minimise f over D. For every call to f in the outer loop a multi-start algorithm with a Sequential Quadratic Programming (SQP) local search and a Latin hypercube initialisation with 3 random samples is used to maximise f in the inner-loop. Table 1 summarizes the decision space D, and optimisation parameters for impulsive strategies (NED, KI) and slow-push strategies (LA, GT, IBS), including the number of agents per population (agents), the number of population (population) and the total number of calls to the objective function (fevals). SQP is performed by $fmincon$ function in MATLAB with the tolerance of $1e^{-6}$.

3. Intelligent Decision Support System

The Intelligent Decision Support System (IDSS) proposed in this paper classifies deflection technologies according to their ability to achieve a minimum probability of collision under epistemic uncertainty. Each deflection method is classified either as successful

Table 1: Optimisation parameters for MP-AIDEA.

Strategy	**Time of transfer** [$years$]	**Time of mission** [$years$]	**Agents**	**Population**	**Fevals**
Impulsive	[1, 4]	[4, 10]	10	4	90
Slow-push	[1, 7]	[7, 10]	10	4	60

or unsuccessful given all the pieces of evidence on the values of the epistemic parameters. The classifier associated to each deflection method is trained on the same set of virtual impact scenarios. Each scenario is defined by the warning time, the orbital elements of the NEO, its mass and the associated uncertainties (see Figure 1). For each virtual impact scenario and deflection technology an optimal launch, orbit transfer and robust deflection action are computed by solving problem (40). The resulting value of P_c' is then used to classify the deflection technology. All computations are performed using a 3.2GHz AMD Ryzen 7 5800H and 16GB of RAM, equipped with MATLAB and Python.

The IDSS is trained on a synthetic data-set composed of variety of possible impact scenarios and deflection outcomes. The variety and diversity of the impact scenarios (both impact geometries and type of NEO) is essential to properly train the IDSS. The fidelity of the deflection outcome is dependent on the fidelity of the model of the deflection actions and associated technology. Since there are no available data on actual NEO deflections or impact scenarios, the IDSS is trained to account also for the existing epistemic uncertainty on both the probability of impact and the deflection outcome.

At this point it is worth noting that while the IDSS presented in this paper is only returning the list of applicable deflection technologies, the classifiers are trained on a data-set that contains also the optimal deflection missions. Thus the same data-set can be used to train a further ML model that can return the optimal mission. The data-set can also be enriched with higher fidelity simulations of the deflection methods. Furthermore, in this paper we considered only a small number of uncertainty sources that do not include the epistemic uncertainty on the deflection technology itself and a number of physical properties of the NEO. If these additional epistemic uncertainties were considered, the IDSS would allow multiple assessments of the deflection methods without recomputing a robust optimisation of the whole deflection mission. These two extensions will be the subject of future work. The scope of this paper is to introduce the methodology and show its applicability to some illustrative cases. For this reason we limited the complexity of the uncertainty and deflection models.

3.1. Data-set Generation

This section explains how we generated the data-set to train the machine learning model. The procedure involves three main steps: the first step is to generate a variety of Virtual Impactors (VIs) with different close encounter geometries in order to cover as many possible future scenarios as possible, the second step is to apply uncertainties to virtual impactors to form the virtual impact scenarios, and the third step is to perform the robust optimisation for each virtual impact scenarios and label the resulting probability of collision.

Step1 (generate virtual impactors): we assume the Earth orbit is circular, therefore, two necessary but not sufficient conditions on the semi-major axis a, eccentricity e for virtual impactors are

$$\begin{cases} a\,(1-e) < 1\text{AU} \\ a\,(1+e) > 1\text{AU} \end{cases} \tag{41}$$

Fixing the semi-major axis a, eccentricity e and inclination i with Near Earth Object's actual value from the JPL Small-Body Database, one independent element remaining to fix is the longitude of the ascending node node Ω of the asteroid's orbital plane with respect to the ecliptic plane. However, since the assumption of circular Earth orbit, the expected impact epoch t_{MOID} (time of Minimum Orbit Intersection Distance, MOID) is arbitrary and we can choose to fix $\Omega = 0$. The argument of perihelion ω and the

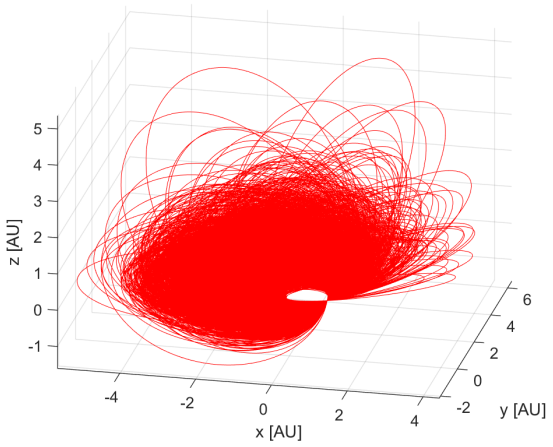

Fig. 2: Trajectories of VIs.

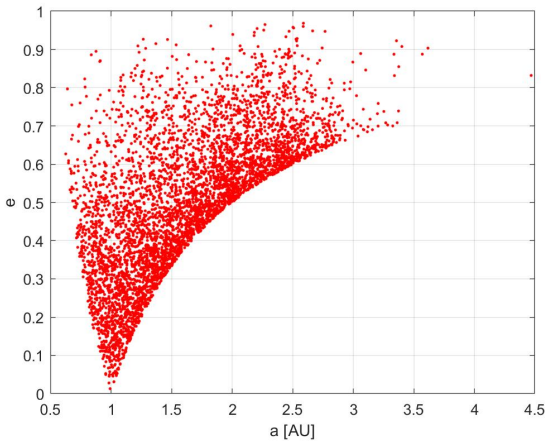

Fig. 3: Distribution in semi-major axis and eccentricity of VIs.

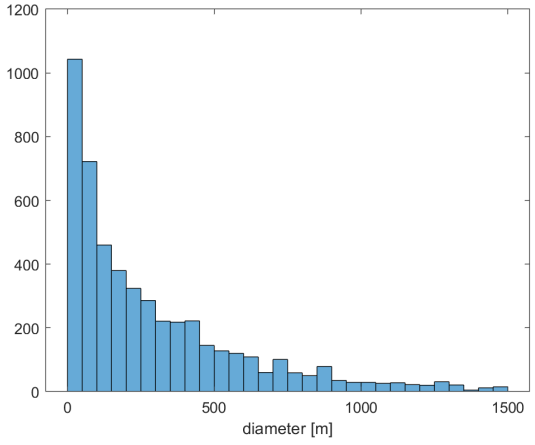

Fig. 4: Histogram of VIs' diameter.

true anomaly θ are determined by Thiry & Vasile (2017)

$$\begin{cases} 1\text{AU} = \frac{a(1-e^2)}{1+e\cos\omega} \\ \theta = 2\pi - \omega \end{cases} \tag{42}$$

11,619 asteroids pass the above filters and form the VIs. We randomly select 5000 of them to apply the uncertainties on orbital elements $\boldsymbol{æ}$ and absolute visual magnitude H, which further form the virtual impact scenarios. Figure 2 and Figure 3 show the trajectories and $a-e$ distribution of 5000 VIs. Meanwhile, the corresponding absolute visual magnitude H values are downloaded from JPL Small-Body Database. Figure 4 shows the histogram of VIs' diameter.

Step2 (apply uncertainties on virtual impactors): To get the reasonable uncertainties intervals ($[\underline{\sigma}, \overline{\sigma}]$) of $\boldsymbol{\sigma}_{\boldsymbol{æ}}$ and σ_H, we count the distribution of real $\boldsymbol{\sigma}_{\boldsymbol{æ}}$ and σ_H from the JPL Small-Body Database Browser, then two reasonable uncertainty intervals for $\boldsymbol{\sigma}_{\boldsymbol{æ}}$ and σ_H are summarized in Table 2. For each VI, the warning time are randomly collected from [5, 10] years and uncertainty intervals e_{ij} are the random subsets collected from the uncertainty intervals Λ_{ij} listed in Table 2, that is

$$\{e_{ij} | e_{ij} \subset \Lambda_{ij},\ i = 1, 2, ..., 7; j = 1, 2\} \tag{43}$$

Finally, a total of 5,000 virtual impact scenarios are generated.

Step3 (perform robust optimisation and label the outcome): For each virtual impact scenario, we perform a robust optimisation,

Table 2: Uncertainty Intervals of $\boldsymbol{\sigma_{\mathbf{xe}}}$ and σ_H. Two sources of the uncertainty intervals are considered: Source1 indicates smaller uncertainty intervals, and Source2 indicates lager uncertainty intervals.

Parameters	**Source1** $\boldsymbol{\Lambda_{.1}}$	**Source2** $\boldsymbol{\Lambda_{.2}}$
$\sigma_a[AU]$	[1e-10, 1e-6]	[1e-6, 1e-1]
σ_e	[1e-8, 1e-6]	[1e-4, 1e-2]
σ_i [°]	[1e-6, 1e-4]	[1e-3, 1e-1]
σ_Ω [°]	[1e-5, 1e-3]	[1e-3,1e-1]
σ_ω [°]	[1e-5, 1e-3]	[1e-3, 1e0]
σ_M [°]	[1e-5, 1e-3]	[1e-2, 1e0]
σ_H	[0.1, 0.5]	[0.5, 0.8]

under mixed aleatory and epistemic uncertainties, of the deflection scenario with five different deflection strategies. We then compute the worst probability of collision

$$P'_{c(max)} = \max_{\overline{\boldsymbol{u}} \in \overline{U}} f\left(\boldsymbol{d}^*, \overline{\boldsymbol{u}}\right) \tag{44}$$

where $\boldsymbol{d}^*$ is the robust solution of problem (40). Figure 5 shows the worst deflection effectiveness $P'_{c(max)}$ of five different deflection strategies within 10 years warning time, where the x, y, z axis indicate the semi-major axis, eccentricity and diameter of the VIs respectively. The $P'_{c(max)}$ will be used to determine whether the execution of deflection is successful.

In this paper, a 'successful deflection' is defined as a deflection such that the worst probability of collision $P'_{c(max)}$ is below 10^{-2}, that is:

$$\forall \boldsymbol{u} \in U, \quad P'_{c(max)} < 10^{-2} \tag{45}$$

In other words, once the $P'_{c(max)}$ of a certain deflection strategy is less than 10^{-2}, the deflection strategy will be labeled as 'successful', otherwise it will be labeled as 'un-successful'. Figure 6 shows the percentage of the scenarios (among 5000 virtual impact scenarios) that can be successfully deflected (the ones labeled with 'successful') by five different deflection strategies, while 'None' indicates that none of the deflection strategies can achieve the successful deflection. Simulation results show that 81.48% of the scenarios can be deflected successfully by NED, 23.6% by KI, 19.28 % by LA, 2.6% by GT and 8.4 % by IBS, while 17.82% of the scenarios cannot be deflected successfully by any strategies within 10 years warning time. Besides NED strategy, KI and LA strategies are mostly likely be selected for the scenarios within 10 years warning time.

3.2. Machine Learning Model

In the following we will use a Random Forest (RF) technique, which was proven to work very well on a similar classification task related to debris conjunction analysis Fernández-Mellado & Vasile (2021), to train the five classifiers. RF is an ensemble method that combines several independent Decision Trees during the training process, which overcome the overfitting problem usually faced by Decision Trees. In this paper, RF is implemented by using the available packages included in Python's Scikit library. The hyperparameters are setting as follows: the models differed in the number of trees in the forest is (50, 100, 200, 400); the maximum depth of the tree is ('None', 50, 100); the minimum number of samples required to be at a leaf node is (1, 10^{-4}, 10^{-7}); the minimum number of samples to split a node is (2, 20); the number of features to consider when looking for the best split is ('auto',0.5,'log2'). For each classifier, we use 80% of the samples for training and 20% for testing. The mean value of F1-score is employed to assess the model, while the definitions of overall accuracy, recall, precision, F1-score are

$$accuracy = \frac{TP + TN}{TP + TN + FP + FN} \tag{46}$$

$$recall = \frac{TP}{TP + FN} \tag{47}$$

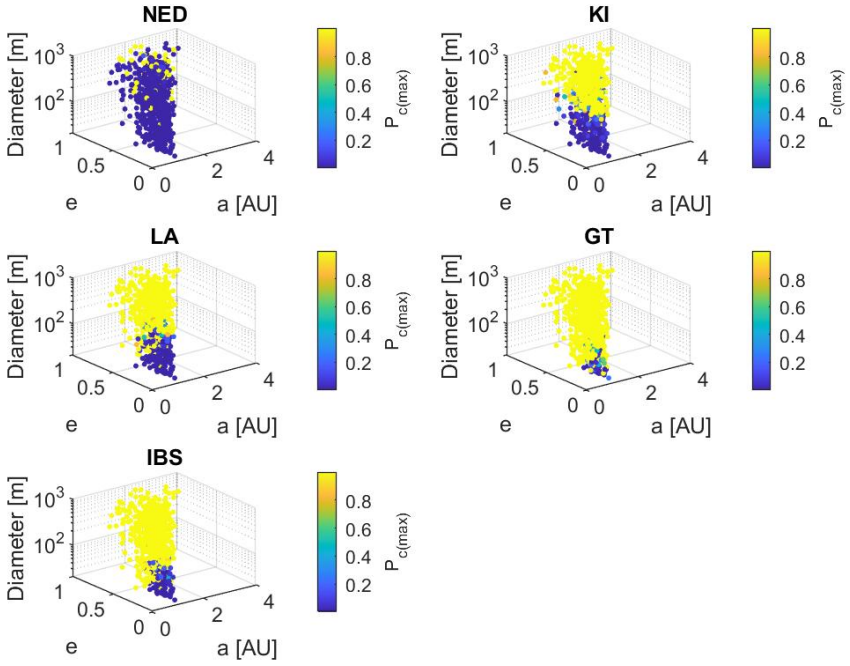

Fig. 5: Five deflection strategies' worst deflection effectiveness $P'_{c(max)}$ within 10 years warning time. The points that tend to be blue in color indicate the lower $P'_{c(max)}$, to some extent, symbolize the virtual impact scenarios that can be successfully deflected.

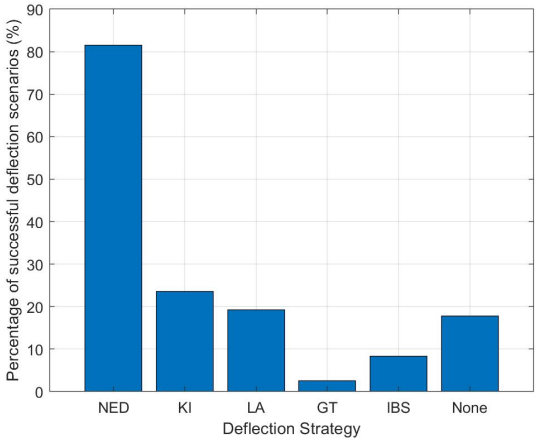

Fig. 6: Percentage of the scenarios that can be deflected successfully. With the warning time less than 10 years, NED is the most powerful strategy that can defend over 80% asteroid impact scenarios, while the GT is the weakest strategy that can only defend 2.6% asteroid impact scenarios.

Table 3: Classification results of five sub-classifiers of IDSS. The accuracy, recall, precision and F1 are used to evaluate the performance of each sub-classifier.

Classifier	Class	Accuracy [%]	Recall [%]	Precision [%]	F1 [%]
NED Classifier	Overall	**88.4**			**75.01**
	un-successful		44.19	79.17	56.72
	successful		97.58	89.38	93.3
KI Classifier	Overall	**95.6**			**93.5**
	un-successful		96.95	97.44	97.19
	successful		90.65	88.99	89.81
LA Classifier	Overall	**96.2**			**92.97**
	un-successful		99.51	96.02	97.74
	successful		80.68	97.26	88.2
GT Classifier	Overall	**97.4**			**61.11**
	un-successful		100	97.39	98.68
	successful		13.33	100	23.53
IBS Classifier	Overall	**95.8**			**80.47**
	un-successful		100	95.64	97.77
	successful		46.15	100	63.16

$$precision = \frac{TP}{TP + FP} \tag{48}$$

$$F_1 = 2\frac{recall * precision}{recall + precision} \tag{49}$$

where TP: True Positive; FP: False Positive; TN: True Negative; FN: False Negative.

3.3. Performance of Intelligent Decision Support System

By RF technique, the classification results of IDSS are obtained by predicting the labels of samples in the testing set. Table 3 shows the classification results of IDSS. The accuracy of KI Classifier and LA Classifier are 95.6% and 96.2% respectively. Note that the F1 score of NED Classifier, GT Classifier and IBS Classifier shows a lower value compared with the ones of KI Classifier and LA Classifier, this is caused by the imbalance in the current data set. For example, the percentage of the scenarios labeled as 'successful' for GT and IBS are less than 20%. In this case, the recall and precision scores of GT Classifier and IBS Classifier indicate that the 'successful' scenarios for GT and IBS tend to be mislabeled as 'un-successful'. Such imbalanced data set is intrinsic to the deflection scenarios with a NEO diameter less than 1000 m and a warning time less than 10 years. An extended data set, which considers larger NEOs and longer warning times, is needed to improve the performance of the IDSS.

The statistical analysis of the output of the current classifier also implies that the NED technology is reliably classified when successful, however, since there is a small proportion of outputs in which the NED option is classified as unsuccessful even a small percentage of false positives for the label "successful" drives the recall down to 44.19%. A symmetric consideration applies to the GT and IBS because the percentage of times the answer is "successful" is small compared to the false positive labels "unsuccessful". In both cases, however, the total number of correct answers is very high, thus, even with an unbalanced data-set, the IDSS returns the correct answer most of the times.

To intuitively show the performance of IDSS, in the remainder of this section we test IDSS on three cases of virtual impact scenarios. For each case, as described in Eq.(43), two sources of uncertainty intervals for each component are randomly collected from $\Lambda_{\cdot 1}$ and $\Lambda_{\cdot 2}$ listed in Table 2, while two sources are equally reliable:

$$bpa(\Lambda_{\cdot 1}) = bpa(\Lambda_{\cdot 2}) = 0.5 \tag{50}$$

The information and simulation results of the three cases are summarised in Table 4, where Case 1 indicates the Virtual Impactor (VI) with the larger size and easier orbital accessibility, Case 2 indicates the VI with the smaller size and easier orbital accessibility

Table 4: Information and simulation results of three cases for testing the computational efficiency improvement of IDSS. The inputs are the mean value μ and the standard deviation σ of orbital elements and absolute magnitude, as well as the warning time. Two rows of σ intervals for each orbital elements indicate smaller and larger uncertainty intervals randomly drawn from two uncertainty sources in Table2. The computational time of running robust optimisation and ML prediction are reported in the last two rows.

	Case 1		**Case 2**		**Case 3**	
	μ	σ **intervals**	μ	σ **intervals**	μ	σ **intervals**
a [AU]	1.006	[4.01E-9, 9.38E-8]	1.078	[6.04e-8, 8.30e-8]	1.283	[8.08e-8, 8.82e-8]
		[9.01E-4, 9.45E-4]		[1.57e-4, 2.13e-4]		[1.65e-4, 8.31e-4]
e	0.23	[8.25E-7, 9.30E-7	0.159	[6.44e-7, 7.97e-7]	0.452	[5.29e-7, 8.39e-7]
		[6.79E-4, 8.04E-4]		[8.54e-4, 9.49e-4]		[5.17e-4, 8.28e-4]
i [°]	1.599	[3.98E-5, 7.18E-5]	3.035	[6.41e-5, 8.19e-5]	17.128	[3.23e-5, 3.81e-5]
		[2.28E-3, 5.54-3]		[2.75e-3, 5.42e-3]		[5.82e-3, 8.77e-3]
Ω [°]	0	[6.34e-5, 9.99e-5]	0	[5.81e-5, 8.50e-5]	0	[8.06e-5, 8.49e-5]
		[5.07e-3, 9.64e-3]		[3.29e-3, 6.78e-3]		[6.05e-3, 7.11e-3]
ω [°]	101.855	[1.93e-5, 8084e-5]	71.231	[6.99e-5, 9.09e-5]	272.74	[1.21e-5, 3.08e-5]
		[2.51e-3, 7.90e-3]		[1.03e-3, 7.80e-3]		[8.97e-3, 9.34e-3]
M [°]	-75.349	[5.55e-5, 8.70e-5]	-54.712	[2.05e-5, 8.51e-5]	38.162	[7.23e-5, 7.84e-5]
		[7.45e-3, 8.60e-3]		[9.68e-3, 9.98e-3]		[6.32e-3, 7.26e-3]
H	22.7	[0.290, 0.451]	24.4	[0.267, 0.410]	25	[0.470, 0.487]
		[0.780, 0.797]		[0.549, 0.686]		[0.598, 0.692]
Diameter $[m]$	97.67		44.64		33.87	
Warning time $[years]$	8.57		9.47		6.58	
Suggested strategies	NED		NED, KI, LA, IBS		NED, KI	
Computational time for robust solution $[s]$	511.63		752.96		88.97	
Computational time for ML prediction $[s]$	<2		<2		<2	

and Case 3 indicates the VI with the smaller size and harder orbital accessibility. The inputs are the mean value μ and the intervals of the standard deviations σ of the orbital elements and absolute magnitudes, as well as the warning time. For these three cases, the total computational time of robust optimisation (for five deflection strategies) are 511.63s, 752.96s, 88.97s respectively. Once the IDSS is used to predict the suggested strategies, the total computational time for each case can be reduced to less than 2s, while the prediction results are the same as the results from robust optimisation. Table 4 shows a reduction of nearly three orders of magnitude in the computational time to assess the effectiveness of a group of deflection technologies. This reduction is proportional to the total mission duration and is expected to further increase as more uncertainty and higher fidelity models are considered in the prediction.

For these three cases, the corresponding belief curves of five deflection strategies are shown in Figure 7a - Figure 7c. It is shown that the difference between different strategies' belief curves becomes more obvious as the asteroid's diameter decreases. For Case 1, note that the left-side of belief curves of KI/LA/GT/IBS are almost unchanged, this is caused by the large σ_a collected from Source2 in Table 2. Taking one focal element that includes the σ_a collected from Source2 as an example, Figure 8 gives the 3-σ ellipses (on the B-plane) corresponding to the best case $P'_{c(min)}$ and the worst case $P'_{c(max)}$. The Case 1's VI has a diameter of 97m, which is not that big but when considering large uncertainty intervals, the effect of large uncertainties on P'_c makes the effect of deflection strategies negligible. Although Source2 intervals selected for Case 2 and Case 3 are also large, the smaller size of Case 2 and Case 3 makes the effect of deflection strategies more obvious. For Case 3, which is hard for spacecraft to rendezvous with, Figure 7c shows that NED and KI outperform slow-push strategies, at the same time, a slight advantage of LA is shown among the slow-push strategies due to the fact that LA does not require to carry as much propellant on board, as IBS and GT, to deflect the NEO.

Note that a NED for small asteroid might not be a recommended solution for other reasons than the pure deflection efficiency. In this paper we did not include additional constraints and considerations which would be required to select the nuclear option vs. non-nuclear solutions. Factors, related to the reliability or controllability of a deflection action can be included in the uncertainty

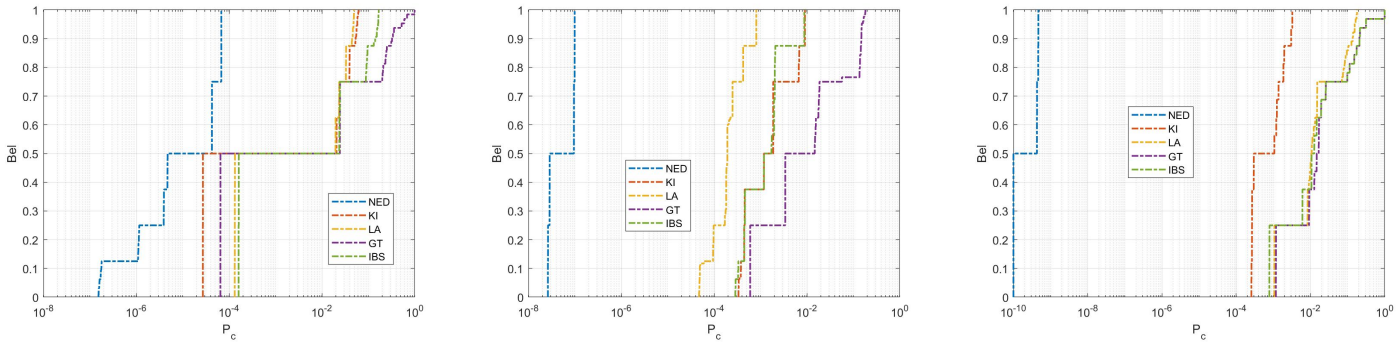

(a) (b) (c)

Fig. 7: Belief curves of five deflection strategies: a) Case1, the VI with the larger size and easier orbital accessibility,; b) Case2, the VI with the smaller size and easier orbital accessibility; c) Case3, the VI with the smaller size and easier orbital accessibility

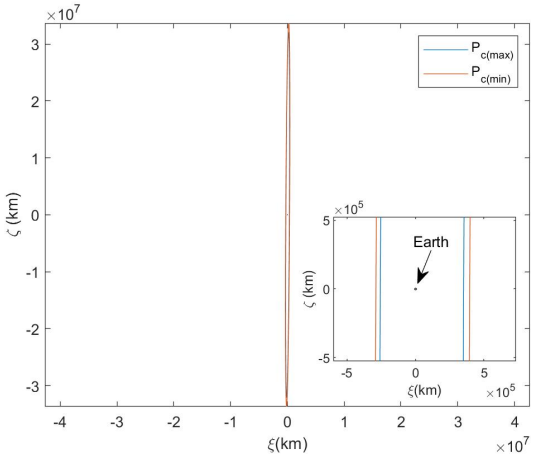

Fig. 8: Case1's 3-σ ellipses of $P_{c(min)}$ and $P_{c(max)}$ on B-plane, where the tiny black circle indicates Earth.

model, in the deflection model or both.

4. Conclusion

This paper has proposed an Intelligent Decision Support System (IDSS), which can automatically assess the effectiveness of deflection strategies at responding to an asteroid impact scenario. The IDSS combines a Machine Learning model with DSt to make robust decisions on the applicable deflection technologies. The ML model is built by training a Random Forest on thousands of virtual impact scenarios and optimised deflection actions. The paper demonstrated how the IDSS can classify the applicability of different deflection technologies, given the type of NEO, the geometry of the expected impact and the uncertainty associated to it. The IDSS can return the list of applicable technologies without the need of expensive simulations and mission optimisations. This list can give a first indication of which strategies should be selected under the considered mixed aleatory and epistemic uncertainty. Thus the IDSS can be used to provide a rapid screening of all deflection options at an early stage of the decision making process and multiple fast re-assessment of a given technology once more information is available. The IDSS can also be used to assess the applicability of different technologies to a catalogue of NEOs and to quickly repeat the assessment when the impact risk in the catalogue is updated.

The results in this paper are preliminary but demonstrate the potentiality of the combination of Dempster-Shafer theory of evidence and machine learning to make informed decisions under mixed uncertainty on the most suitable deflection options in the case of a threatening scenario. This work included only uncertainty on the mass of the asteroid and its ephemerides. A more complete treatment would require the inclusion of uncertainty on the deflection action and on other physical properties of the asteroid. This is

a critical aspect of the effectiveness and applicability of all deflection methods. The inclusion of uncertainty on the deflection action and its sensitivity to the properties of the asteroid would change the classification in favour of more reliable methods.

Furthermore the only criterion used to classify is the probability of collision. This would need to be complemented by possible operational or implementation constraints and more general considerations on technology readiness and viability. Finally the data-set used to train the classifiers contains a lot more information on the mission profile, trajectory, transfer manoeuvres, launch date, etc. In the current version of the IDSS this information is not returned but can be used to train a further model associated to the classification of the technology so that an optimal mission is returned together with the associated technology. All these extensions will be the subject of future work.

5. Acknowledgments

This work was supported through the Horizon 2020 MSCA ETN Stardust-R (grant agreement number: 813644). The authors express their gratitude to Luis Sanchez Fernandez-Mellado for his help in implementing the Patera's method and Random Forest.

References

Bambacus, M., Yang, C. P., Leung, R. Y. et al. (2017). A planetary defense gateway for smart discovery of relevant information for decision support. In *IAA Planetary Defense Conference* GSFC-E-DAA-TN42303.

Bombardelli, C., Urrutxua, H., Merino, M. et al. (2013). The ion beam shepherd: A new concept for asteroid deflection. *Acta Astronautica*, *90*(1), 98–102. URL: https://www.sciencedirect.com/science/article/pii/S0094576512003979. doi:https://doi.org/10.1016/j.actaastro.2012.10.019. NEO Planetary Defense: From Threat to Action - Selected Papers from the 2011 IAA Planetary Defense Conference.

Chesley, S. R., Chodas, P. W., Milani, A. et al. (2002). Quantifying the risk posed by potential earth impacts. *Icarus*, *159*(2), 423–432.

Dearborn, D. S., Syal, M. B., Barbee, B. W. et al. (2020). Options and uncertainties in planetary defense: Impulse-dependent response and the physical properties of asteroids. *Acta Astronautica*, *166*, 290–305.

Di Carlo, M., Vasile, M., & Minisci, E. (2020). Adaptive multi-population inflationary differential evolution. *Soft Computing*, *24*(5), 3861–3891.

Fernández-Mellado, L. S., & Vasile, M. (2021). On the use of machine learning and evidence theory to improve collision risk management. *Acta Astronautica*, *181*, 694–706.

Julier, S. J., Uhlmann, J. K., & Durrant-Whyte, H. F. (1995). A new approach for filtering nonlinear systems. In *Proceedings of 1995 American Control Conference-ACC'95* (pp. 1628–1632). IEEE volume 3.

Lu, E. T., & Love, S. G. (2005). Gravitational tractor for towing asteroids. *Nature*, *438*(7065), 177–178.

Luo, Y.-z., & Yang, Z. (2017). A review of uncertainty propagation in orbital mechanics. *Progress in Aerospace Sciences*, *89*, 23–39.

Nesvold, E., Greenberg, A., Erasmus, N. et al. (2018). The deflector selector: A machine learning framework for prioritizing hazardous object deflection technology development. *Acta Astronautica*, *146*, 33–45. URL: https://www.sciencedirect.com/science/article/pii/S0094576517313747. doi:https://doi.org/10.1016/j.actaastro.2018.01.049.

Novak, D. M., & Vasile, M. (2011). Improved shaping approach to the preliminary design of low-thrust trajectories. *Journal of guidance, control, and dynamics*, *34*(1), 128–147.

Paek, S. W., de Weck, O., Hoffman, J. et al. (2020). Optimization and decision-making framework for multi-staged asteroid deflection campaigns under epistemic uncertainties. *Acta Astronautica*, *167*, 23–41.

Patera, R. P. (2001). General method for calculating satellite collision probability. *Journal of Guidance, Control, and Dynamics*, *24*(4), 716–722.

Raskin, C., Remington, T., & Owen, M. (2021). Accelerated root finding for the dart inverse test using machine learning decision trees. In *7th IAA Planetary Defense Conference* (p. 51).

Sanchez, J. P., Colombo, C., Vasile, M. et al. (2009). Multicriteria comparison among several mitigation strategies for dangerous near-earth objects. *Journal of Guidance, Control, and Dynamics*, *32*(1), 121–142.

Schaub, H., & Junkins, J. L. (2003). *Analytical mechanics of space systems*. AIAA, Reston.

Shafer, G. (1976). *A mathematical theory of evidence*. Princeton university press, Princeton.

Sánchez Fernández-Mellado, L., & Vasile, M. (2021). On the use of machine learning and evidence theory to improve collision risk management. *Acta Astronautica*, *181*, 694–706. URL: https://www.sciencedirect.com/science/article/pii/S0094576520304914. doi:https://doi.org/10.1016/j.actaastro.2020.08.004.

Thiry, N., & Vasile, M. (2017). Statistical multi-criteria evaluation of non-nuclear asteroid deflection methods. *Acta Astronautica*, *140*, 293–307.

Vasile, M. (2002). Robust optimisation of trajectories intercepting dangerous neo. In *AIAA/AAS Astrodynamics Specialist Conference and Exhibit* (p. 4719).

Vasile, M., & Colombo, C. (2008). Optimal impact strategies for asteroid deflection. *Journal of guidance, control, and dynamics*, *31*(4), 858–872.

Vasile, M., Minisci, E., Zuiani, F. et al. (2011). Fast evidence-based space system engineering. In *62nd International Astronautical Congress* (pp. 1–12).

Vasile, M., & Thiry, N. (2016). Nuclear cycler: An incremental approach to the deflection of asteroids. *Advances in Space Research*, *57*(8), 1805–1819.

Weisbin, C., Lincoln, W., Wilcox, B. et al. (2015). Comparative analysis of asteroid-deflection approaches. In *2015 IEEE Aerospace Conference* (pp. 1–16). IEEE.

366 Yamaguchi, T., Kogiso, N., & Yamakawa, H. (2008). Optimal interplanetary trajectories for impulsive deflection of potentially hazardous asteroids under velocity
367 increment uncertainties. *Transactions of the Japan Society for Aeronautical and Space Sciences*, *51*(173), 176–183.
368 Zuiani, F., Vasile, M., & Gibbings, A. (2012a). Evidence-based robust design of deflection actions for near earth objects. *Celestial Mechanics and Dynamical*
369 *Astronomy*, *114*(1), 107–136.
370 Zuiani, F., Vasile, M., Palmas, A. et al. (2012b). Direct transcription of low-thrust trajectories with finite trajectory elements. *Acta Astronautica*, *72*, 108–120.